JACS
JOURNAL OF THE AMERICAN CHEMICAL SOCIETY
Article
Cite This: J. Am. Chem. Soc. 2019, 141, 10475−10480
pubs.acs.org/JACS

# Triphenylene-Bridged Trinuclear Complexes of Cu: Models for Spin Interactions in Two-Dimensional Electrically Conductive Metal−Organic Frameworks

Luming Yang,[†] Xin He,[†] and Mircea Dincă*

Department of Chemistry, Massachusetts Institute of Technology, 77 Massachusetts Avenue, Cambridge, Massachusetts 02139, United States

Supporting Information

**ABSTRACT:** Reaction of 2,3,6,7,10,11-hexahydroxytriphenylene (HHTP) and 2,3,6,7,10,11-hexaaminotriphenylene (HATP) with $[Cu(Me_3tacn)]^{2+}$ ($Me_3tacn$ = 1,4,7-trimethyl-1,4,7-triazacyclononane) produces trigonal tricopper complexes $[(Me_3tacnCu)_3(HOTP)]^{3+}$ (**1**) and $[(Me_3tacnCu)_3(HITP)]^{4+}$ (**2**) (HOTP, HITP = hexaoxy- and hexaiminotriphenylene, respectively). These trinuclear complexes are molecular models for spin exchange interactions in the two-dimensional conductive metal−organic frameworks (MOFs) copper hexaoxytriphenylene ($Cu_3HOTP_2$) and copper hexaiminotriphenylene ($Cu_3HITP_2$). Whereas complex **1** is isolated with $HOTP^{3-}$ bearing the same oxidation state as found in the oxy-bridged MOF, the triply oxidized $HITP^{3-}$ found in $Cu_3HITP_2$ is unstable with respect to disproportionation in the molecular model. Indeed, magnetic measurements reveal ligand-centered radical character for **1** and a closed-shell structure for **2**, in agreement with the redox state of the ligands. All neighboring spins are antiferromagnetically coupled in **1** and **2**. These results help probe metal−ligand−metal interactions in conductive MOFs and provide potential inspiration for the synthesis of other two-dimensional materials with delocalized electrons.

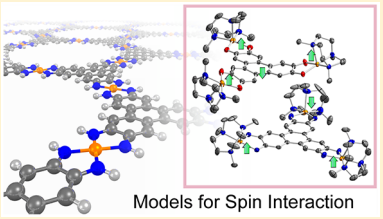


## INTRODUCTION

Multifunctional spintronic devices that respond to electrical, magnetic, and chemical stimuli have drawn much attention in recent years due to their important role in downsizing logic circuits.[1−3] One class of materials that show promise toward such applications are two-dimensional (2D) electrically conductive metal−organic frameworks (MOFs) made from paramagnetic ions that in principle respond to electrical, magnetic, as well as chemical stimuli.[4−17] These 2D MOFs have layered graphene-like honeycomb structures, where the vertices in the hexagonal tiles are the tritopic organic ligands and the transition metals ions bridging the ligands reside on the edges of each hexagon (Figure 1).[4,10,17] Because the ligands and metals in MOFs can be independently modified or chosen, these materials present opportunities that are not easily achieved with graphite or other 2D materials, allowing for control over porosity, conductivity, and spin state. However, the extended structures and compositional complexity also translate into complicated electronic structures that give rise to electrical and magnetic properties that are still poorly understood despite numerous experimental and computational studies.[8,9,18−20] One powerful means to interrogate the properties of solids has been dimensional reduction, wherein the independent synthesis and study of smaller building blocks provide insight into the electronic structure of the parent solids.[21,22] The 2D conductive materials described above make excellent targets for this strategy. Here, we report trinuclear Cu complexes bridged by the same trigonal ligands found in the MOFs and study their redox and magnetic properties.

## RESULTS AND DISCUSSION

In a manner mimicking the isolation of small clusters related to Prussian blue analogues,[23] we employed $Cu^{2+}$ complexes capped with the neutral multidentate $\kappa_3$-chelating ligand 1,4,7-trimethyl-1,4,7-triazacyclononane ($Me_3tacn$) to target the MOF model complexes. Importantly, the typical coordination mode of $Me_3tacn$ keeps the copper magnetic orbital ($d_{x^2-y^2}$) in the aromatic plane of the ligand, as is also likely the case in $Cu_3HXTP_2$ (X = O, I). Because in the extended MOFs the ligand is formally triply oxidized—and thus bears a formal oxidation state of −3 after 6-fold deprotonation of the amino or hydroxy groups—we targeted the same oxidation state in the molecular complexes (Scheme 1, left). In view of the expected rich redox reactivity of $[M_3HOTP]^{n+}$ complexes,[24−26] the target compounds $[(Me_3tacnCu)_3(HXTP)]^{n+}$ were synthesized under inert atmosphere followed by stoichiometric oxidations with 3 equiv of oxidants. Thus, reaction of $[(Me_3tacn)Cu](BF_4)_2$ with 2,3,6,7,10,11-hexahydroxytriphenylene (HHTP) under $N_2$, followed by deprotonation and oxidation with 3 equiv of ferrocenium tetrafluoroborate ($FcBF_4$) yielded $[(Me_3tacnCu)_3(HOTP)](BF_4)_3$ (**1**·$(BF_4)_3$) as dark navy crystals in 73% yield (Scheme S1). Unexpectedly, a similar procedure utilizing 2,3,6,7,10,11-hexaaminotriphenylene (HATP) instead of HHTP did not lead to the isolation of the desired $[(Me_3tacnCu)_3(HITP)]^{3+}$ complex. Instead, upon

**Received:** May 5, 2019
**Published:** June 10, 2019






DOI: 10.1021/jacs.9b04822
J. Am. Chem. Soc. 2019, 141, 10475−10480

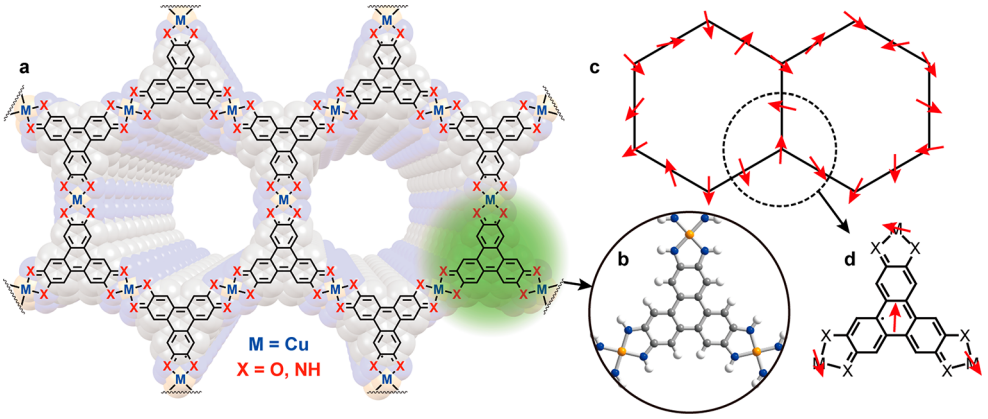


**Figure 1.** (a) Structural and chemical representation of typical 2D conductive MOFs, with depiction of the graphite-like honeycomb structure as well as HXTP (X = O, I) ligand-centered radical. The highlighted part illustrates the trinuclear metal−ligand monomeric unit modeled here as shown in (b). (c) Spin−lattice of typical 2D conductive MOFs, with arrows showing randomized spin centers. (d) Spin structure of the monomeric unit depicted in (b), showing metal- and ligand-centered radicals.

**Scheme 1. Lewis Structures of Selected Resonance Forms of 1 and 2, Illustrating the Charge States and Spin Structures of HXTP (X = O, I), Respectively**[a]

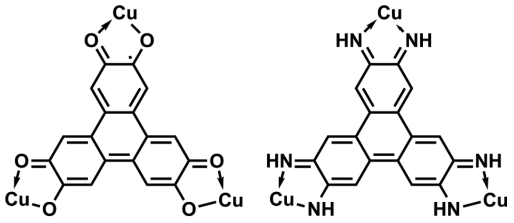


[a]The capping $Me_3tacn$ ligands are omitted for clarity.

reaction of HATP with $[(Me_3tacn)Cu]^{2+}$ and oxidation by 3 equiv of $FcBF_4$, an initially dark blue-green solution changes to a dark blue solution whereupon only $[(Me_3tacnCu)_3(HITP)](BF_4)_4$ ($\mathbf{2}\cdot(BF_4)_4$) could be isolated (Scheme 1, right; also Scheme S1). This more electron-deficient species containing the quadruply oxidized ligand $HITP^{2-}$ suggests that $[(Me_3tacnCu)_3(HITP)]^{3+}$ is unstable with respect to disproportionation, a redox behavior that diverges from that of $Cu_3HITP_2$ under otherwise similar synthetic conditions. The identities of **1** and **2** were confirmed by high-resolution electrospray ionization/mass spectrometry (ESI/MS) and microelemental analyses. The former gave $m/z$ values of 1285.3 for **1** ($[M + H]^+$, M = $[(C_9H_{21}N_3Cu)_3(C_{18}H_6O_6)](BF_4)_3$) and $m/z$ = 1366.4 for **2** ($[M + H]^+$, M =

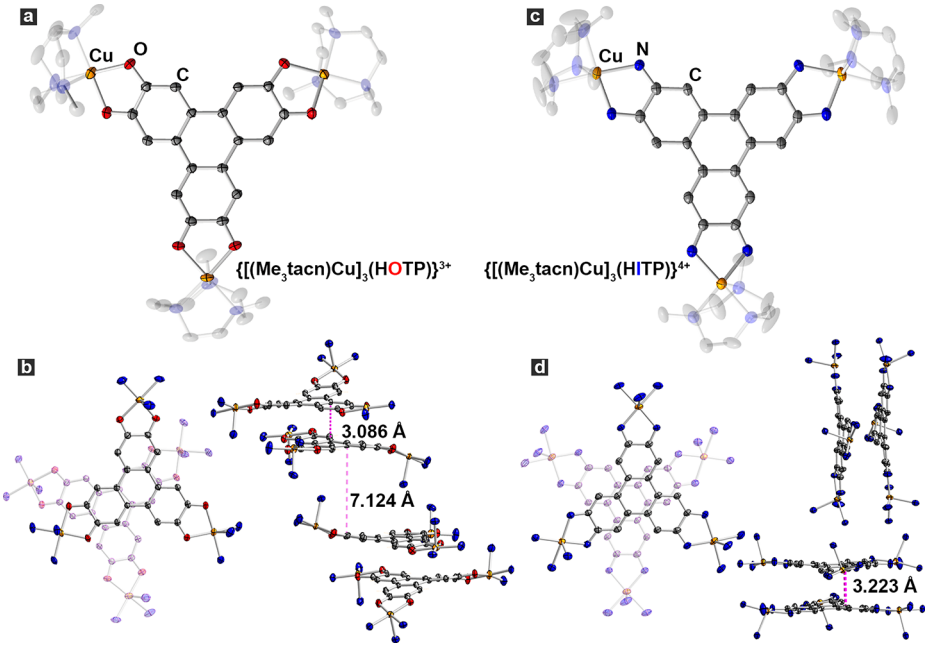


**Figure 2.** Crystal structures of **1** and **2**, showing (a, c) single cationic fragments containing $Cu_3HXTP$ motifs; (b, d) top (left) and side (right) views of the dimeric packing modes in unit cells. Thermal ellipsoids are plotted at 50% probability level for elements other than hydrogen. All anions and solvent molecules are omitted for clarity. The $Me_3tacn$ backbones are also omitted in (b) and (d). The red dotted lines indicate selected intermolecular C···C distances.



DOI: 10.1021/jacs.9b04822
J. Am. Chem. Soc. 2019, 141, 10475−10480

$[(C_9H_{21}N_3Cu)_3(C_{18}H_{12}N_6)](BF_4)_4$, see also Supporting Information).

Single crystals of **1** and **2** suitable for X-ray diffraction (XRD) analysis were obtained by layering or diffusing vapors of *t*-butyl-methyl-ether to solutions of the respective complexes in 4:1 mixtures of dichloroethane:methanol at −5 °C. Compounds **1** and **2** crystallize in space groups $P\bar{1}$ and $P2_1/c$, respectively (Figure 2a,c). In the solid state, both **1** and **2** pack in dimeric fashion, with closest C···C distances of 3.086(5) and 3.223(6) Å between the dimers (Figure 2b,d; right). A top-down view of the dimers reveals staggered conformations for both complexes (Figure 2b,d). In both **1** and **2**, the longest $Cu-N_{Me_3tacn}$ bonds are the axial ones, as expected due to the Jahn−Teller distortion, and confirming the coplanarity of the Cu $d_{x^2-y^2}$ magnetic orbital with the HXTP plane. For metal-semiquinone complexes, the C−O bond length is often related to the degree of oxidation of the semiquinone fragment. Shorter C−O bonds indicate more oxidized (quinone-type) character whereas longer C−O bonds correspond to reduced (catechol-type) character.[27] For **1**, the average C−O bond length is 1.283(4) Å, in very good agreement with the value of 1.288(2) Å reported for an established copper bis-semiquinonate complex.[28] In contrast, **2** exhibits an average C−N bond length of 1.305(6) Å, shorter than that of a structurally relevant bis-iminosemiquinonate copper azophenine complex (1.327(3) Å).[29] Although subtle, the difference between the shorter average C−N bond length in **2** relative to the established iminosemiquinonate Cu complex is consistent with a higher degree of oxidation and partial iminoquinone character in **2**.

Cyclic voltammetry (CV) provided further support for assigning formal oxidation states in **1** and **2** and offered clues into the degree of electron delocalization in the trinuclear complexes. CV experiments for complex **1** conducted in 0.1 M propylene carbonate solutions of tetrabutylammonium hexafluorophosphate ($TBAPF_6$) under $N_2$ reveal three reversible reduction events at −0.80, −0.45, −0.09 V relative to the ferrocenium/ferrocene ($Fc^+/Fc$) couple (Figure 3a). All three values are in line with expected ligand-centered redox couples: $HOTP^{3-/4-}$, $HOTP^{4-/5-}$, and $HOTP^{5-/6-}$, the last corresponding to the formation of neutral $[(Me_3tacnCu)_3(HOTP)]$.[25,30] In the framework of the classical theory of mixed-valence compounds, which relates electrochemical redox potentials to the degree of electronic delocalization between mixed-valence centers,[31,32] the potential difference between the $HOTP^{5-/6-}$ and $HOTP^{3-/4-}$couples, $\Delta E$ = 0.71 V, equates to a comproportionation constant,[33] $K_c$, of $10^{12.0}$. This large value indicates that the three redox centers—the three semiquinone/hydroquinone moieties of each HOTP ligand—are fully delocalized and form a Robin-Day class III mixed-valent compound,[34] as may be expected for three formal radicals, all centered on a single organic moiety. A similar analysis for **2** is made difficult by the irreversibility of the first reduction event, presumably the $HITP^{2-/3-}$ couple, which occurs at −0.51 V (Figure 3b). The irreversible reduction of **2** is in line with rapid disproportionation of the $[(Me_3tacnCu)_3(HITP)]^{3+}$ species, which further prevents access to more reduced complexes. Although the strong degree of charge delocalization within HOTP is in-line with the extended delocalization observed in the respective HOTP-based MOF, inaccessible Cu-based redox events with either **1** or **2** prevent the assessment of charge delocalization between the *metal* centers, as mediated by HOTP or HITP.

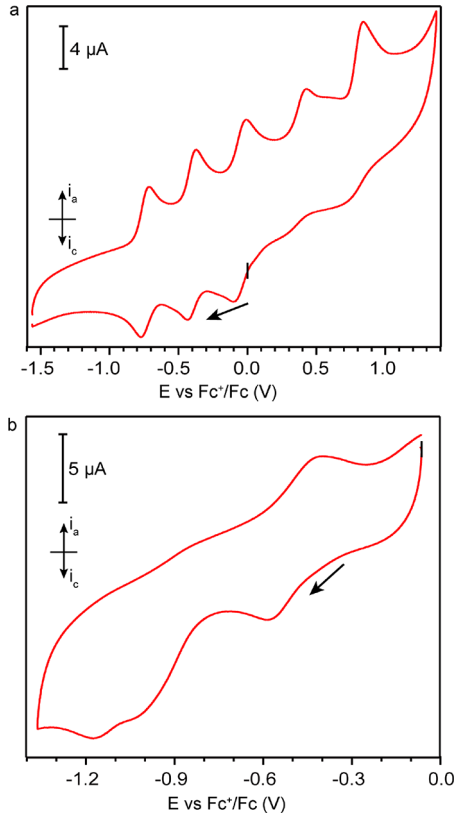


**Figure 3.** Cyclic voltammograms of **1** (a) and **2** (b) in 0.1 M $TBAPF_6$−propylene carbonate under $N_2$. Scanning directions are marked by arrows. Open circuit potentials are indicated by black tick marks.

Magnetometry provided critical information about the electronic communication between metals and/or ligands in complexes **1** and **2**. Variable temperature direct current magnetic susceptibility measurements indicated antiferromagnetic coupling for both complexes, as revealed by rapid decreases of $\chi_M T$ below 50 K in an applied field of 2.5 kOe (Figure 4a). For **1**, a room temperature $\chi_M T$ value of 1.79 $cm^3$ $mol^{-1}$ K is close to the value expected for four independent $S$ = 1/2 spins (1.50 $cm^3$ $mol^{-1}$ K, with $g$ = 2.0), representing three noninteracting $Cu^{2+}$ ions and one $S$ = 1/2 $HOTP^{3-}$ organic radical. Because of a significant contribution from temperature independent paramagnetism (TIP) (see Figure S2 and related discussion for assignment of TIP), the room-temperature $\chi_M T$ value for **2** is 2.32 $cm^3$ $mol^{-1}$ K, higher than expected for three uncoupled $Cu^{2+}$ ions connected through the diamagnetic $HITP^{2-}$ (see Figure S3 for $\chi_M T$ vs T plot where the contributions of TIP were corrected for). The plateau $\chi_M T$ value for **2** of 0.42 $cm^3$ $mol^{-1}$ K at 1.8 K is nevertheless close to the value expected for a $S$ = 1/2 spin system (0.375 $cm^3$ $mol^{-1}$ K with g = 2.0). This suggests that the ground spin state of **2** is $S$ = 1/2, as would be expected for three antiferromagnetically coupled $Cu^{2+}$ ions at low temperature.

To assess the magnitude of the spin exchange interactions, the temperature-dependent $\chi_M T$ data were fitted with Heisenberg−Dirac−van Vleck (HDVV) Hamiltonians, $\mathbf{H}_1$ for **1** and $\mathbf{H}_2$ for **2** (see also Figure S4):

$$\mathbf{H}_1 = -2J_1(\mathbf{S}_{Cu1}\mathbf{S}_L + \mathbf{S}_{Cu2}\mathbf{S}_L) - 2J_2\mathbf{S}_{Cu3}\mathbf{S}_L$$



DOI: 10.1021/jacs.9b04822
J. Am. Chem. Soc. 2019, 141, 10475−10480

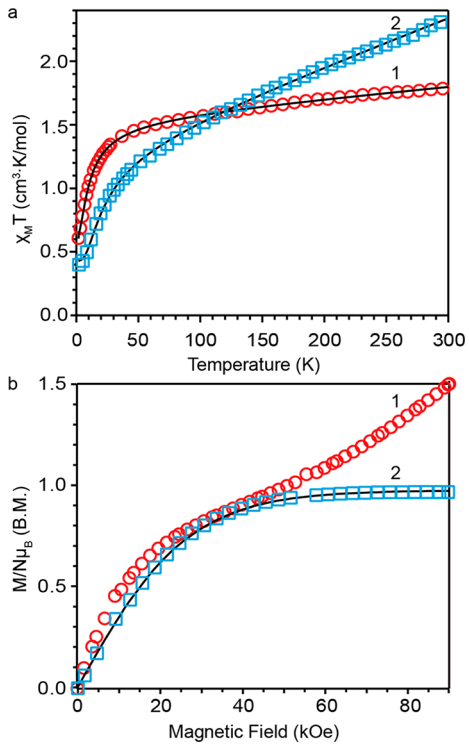


**Figure 4.** (a) Temperature-dependent $\chi_M T$ ($H$ = 2.5 kOe) and (b) field-dependent magnetization ($T$ = 1.8 K) curves for **1** and **2**. The solid black lines are the best fits as described in the text.

$$\mathbf{H}_2 = -2J_1(\mathbf{S}_{Cu1}\mathbf{S}_{Cu2} + \mathbf{S}_{Cu1}\mathbf{S}_{Cu3}) - 2J_2\mathbf{S}_{Cu2}\mathbf{S}_{Cu3}$$

Good fits were obtained for both complexes by using two $J$ values representing only the spin interactions between nearest neighbors. For **1**, fitting with contribution from TIP and intermolecular coupling, $zJ'$, as well as two $g$ values for copper- and ligand-centered spins gives $J_1 = J_2 = -2.76$ cm$^{-1}$ (with $g_{Cu} = 2.06$, $g_L = 1.98$, $\chi_{TIP} = 8.86 \times 10^{-4}$ cm$^3$ mol$^{-1}$, $zJ' = -0.309$ cm$^{-1}$) (Figure 4a) (see Figure S5 and related discussion on the choice of $g$). This indicates that the ligand-based radical is coupled to the three $Cu^{2+}$ ions through weak antiferromagnetic interactions of similar strength. As such, the ground spin state of **1** is $S$ = 1, with the trigonal symmetry preserved in the spin structure despite a geometric distortion from perfect planarity. For **2**, the best fit of the temperature-dependent $\chi_M T$ data gave $J_1 = J_2 = -6.99$ cm$^{-1}$, with $g_{Cu} = 2.12$ and $\chi_{TIP} = 3.71 \times 10^{-3}$ cm$^3$ mol$^{-1}$ (Figure 4a). To assess the possibility that paramagnetic impurities contribute to the magnetic properties of **1** and **2**, we fitted the data by adding $S$ = 1/2 $Cu^{2+}$ impurities. This produced fits with similar parameters as for the pure samples above, with negligible contribution from the $S$ = 1/2 impurities (Figure S6 and related discussions). The lack of crystalline impurities is also supported by the powder X-ray diffraction analysis for **1** and **2** (see Figure S7 and related discussions).

The ground spin states of complexes **1** and **2** were confirmed by variable field magnetization measurements (Figure 4b). For **1**, the magnetization does not saturate even at 90 kOe and continues to grow after reaching an inflection point of ~1 $\mu_B$ at approximately 40 kOe, a behavior that is typically associated with the presence of low-lying excited spin states.[35] The magnetization curve for **1** further deviates from typical Brillouin behavior, likely because of additional intermolecular antiferromagnetic interactions that lower the expected saturation value of 2 $\mu_B$ for an $S$ = 1 system (see Figure S8 and related discussion in the Supporting Information). In contrast, the magnetization of complex **2** follows typical Brillouin-type behavior and shows a saturation value of 1 $\mu_B$, as expected for an $S$ = 1/2 system. Fitting of this data with a Brillouin function gives $g$ = 2.0, a slightly smaller value than usually observed for $Cu^{2+}$, again likely owing to weak intermolecular antiferromagnetic interactions. Low temperature electron paramagnetic resonance (EPR) provided further insight on the electronic structure of **1** and **2**. For **1**, an isotropic $S$ = 1/2 signal at $g$ = 2.00 and an axial $S$ = 1/2 signal with $g_\parallel = 2.25$, $g_\perp = 2.05$, and hyperfine coupling to $Cu^{2+}$ ($I$ = 3/2) with $A_\parallel \sim 30$ G were observed (Figure S9). This agrees with the observation of single unpaired spins on both HOTP and $Cu^{2+}$ from magnetometry measurements in **1**. For **2**, only an axial $S$ = 1/2 signal with $g_\parallel = 2.25$, $g_\perp = 2.05$ is observed, which gives a good fit with $Cu^{2+}$ hyperfine coupling constants of $A_\parallel = 40$ G and $A_\perp = 413$ G, suggesting the presence of $S$ = 1/2 spins coupled to $Cu^{2+}$ in **2**. This is in good agreement with the magnetometry data that suggests the absence of an HITP-based radical in **2**.

Density functional theory (DFT) calculations carried out for the cationic fragments $[(Me_3tacnCu)_3HOTP]^{3+}$ and $[(Me_3tacnCu)_3HITP]^{4+}$ corroborate magnetometry data and provide further insight into the orbital interactions involved in the spin exchange mechanisms in **1** and **2**. For both complexes, DFT calculations agree with the proposed spin density distribution derived from magnetometry data above. The magnetic orbitals of the copper centers have the same symmetry as the $d_{x^2-y^2}$ atomic orbitals, and lie in the plane of the molecule (Figure 5). For both **1** and **2**, the oxygen and nitrogen atoms of the HXTP (X = O, I) ligands have primarily the same sign of spin density as the copper atoms, suggesting ferromagnetic exchange due to orbital orthogonality. Meanwhile, the dominating antiferromagnetic interaction in both complexes is embodied through spin polarization or antiferromagnetic superexchange mechanisms in the p−$\pi$ systems of the ligands.

Altogether, the structural, electrochemical, and magnetic data support a ligand-based $S$ = 1/2 radical in **1**, which therefore represents a first example of a molecular complex modeling electronic interactions in a conductive MOF, in this case $Cu_3HOTP_2$. Notably, even though other examples of isolable $M_3HXTP$-type complexes (X = O, N, S) exist, none of these show spin density on both the metal and the ligand.[24−26,30,32,36] Although **1** is a truncated model of an idealized single-sheet of $Cu_3HOTP_2$, which to our knowledge has not been accessed yet, if the antiferromagnetic interactions observed in **1** are reproduced in a single sheet of $Cu_3HOTP_2$, the latter may exhibit properties consistent with a conductive 2D ferrimagnet.[20,37] Verifying such rare behavior rests entirely with efforts to generate and exfoliate sufficiently large single crystals of $Cu_3HOTP_2$, an area of ongoing interest in our laboratory.

In the same vein, it should be noted that **2** satisfies the classical geometric spin frustration criterion of $J_1 = J_2 < 0$ in a spin triangle, as proposed by Kahn.[38] Although it has been established that true geometric spin frustration cannot be achieved in molecular complexes due to fast geometric relaxation,[39,40] the type of interactions observed in **2** bring about the possibility of a geometrically frustrated solid state material, where structural relaxation to lower symmetry is


DOI: 10.1021/jacs.9b04822
J. Am. Chem. Soc. 2019, 141, 10475−10480

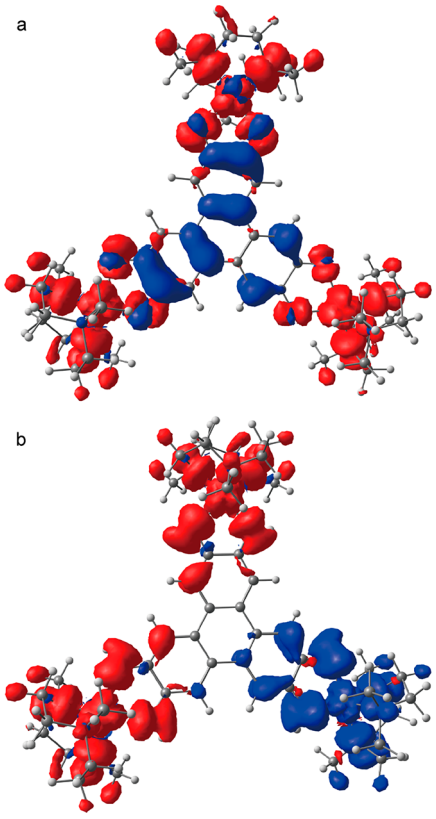


**Figure 5.** Calculated spin density isosurfaces (0.0007 au) of (a) **1** and (b) **2**. Red and blue represent spin-up and spin-down densities.

quenched by lattice rigidity. As with **1**, if it exists, spin frustration is likely to be observed only in single, charged sheets of extended MOFs of the type $M_3(HITP)_2$, with no intersheet interactions.[41,42] Once again, the challenge in accessing such 2D structures rests squarely in the synthetic realm and highlights the importance of controlling crystal growth for 2D conductive MOFs.

## CONCLUSIONS

In conclusion, we present the synthesis, electrochemical, and magnetic characterization of two new trinuclear copper complexes that mimic the smallest building blocks of conductive 2D MOFs $Cu_3HOTP_2$ and $Cu_3HITP_2$. Whereas the oxygen-based complex retains a ligand-based radical similar to the corresponding $Cu_3HOTP_2$, the nitrogen-based ligand radical disproportionates, thereby diverging from the formal oxidation state present in $Cu_3HITP_2$. In both complexes, the metal and/or ligand-based electronic spins are coupled through weak antiferromagnetic interactions. These results portend potentially exciting long-range magnetic interactions in isolated single sheets of the respective 2D MOFs, substantiating the importance of future efforts to isolate such sheets.

## ASSOCIATED CONTENT

### Supporting Information

The Supporting Information is available free of charge on the ACS Publications website at DOI: 10.1021/jacs.9b04822.

X-ray crystal structure of **1** (CIF)
X-ray crystal structure of **2** (CIF)
Details of experimental procedures, single crystal X-ray crystallography, fitting of magnetic data, and computational methods (PDF)

## AUTHOR INFORMATION

### Corresponding Author

*mdinca@mit.edu

### ORCID

Xin He: 0000-0001-8461-8868
Mircea Dincă: 0000-0002-1262-1264

### Author Contributions

†L.Y. and X.H. contributed equally.

### Notes

The authors declare no competing financial interest.

## ACKNOWLEDGMENTS

This work was supported by the Army Research Office (grant number W911NF-17-1-0174). We thank Professor T. David Harris for fruitful discussions.

## REFERENCES

(1) Wolf, S. A.; Awschalom, D. D.; Buhrman, R. A.; Daughton, J. M.; von Molnár, S.; Roukes, M. L.; Chtchelkanova, A. Y.; Treger, D. M. Spintronics: A Spin-Based Electronics Vision for the Future. *Science* **2001**, *294*, 1488−1495.
(2) Awschalom, D. D.; Flatté, M. E. Challenges for Semiconductor Spintronics. *Nat. Phys.* **2007**, *3*, 153−159.
(3) Ballav, N.; Wäckerlin, C.; Siewert, D.; Oppeneer, P. M.; Jung, T. A. Emergence of On-Surface Magnetochemistry. *J. Phys. Chem. Lett.* **2013**, *4*, 2303−2311.
(4) Hmadeh, M.; Lu, Z.; Liu, Z.; Gándara, F.; Furukawa, H.; Wan, S.; Augustyn, V.; Chang, R.; Liao, L.; Zhou, F.; Perre, E.; Ozolins, V.; Suenaga, K.; Duan, X.; Dunn, B.; Yamamto, Y.; Terasaki, O.; Yaghi, O. New Porous Crystals of Extended Metal-Catecholates. *Chem. Mater.* **2012**, *24*, 3511−3513.
(5) Kambe, T.; Sakamoto, R.; Hoshiko, K.; Takada, K.; Miyachi, M.; Ryu, J. H.; Sasaki, S.; Kim, J.; Nakazato, K.; Takata, M.; Nishihara, H. l. π-Conjugated Nickel Bis(Dithiolene) Complex Nanosheet. *J. Am. Chem. Soc.* **2013**, *135*, 2462−2465.
(6) Huang, J.; He, Y.; Yao, M. S.; He, J.; Xu, G.; Zeller, M.; Xu, Z. A Semiconducting Gyroidal Metal-Sulfur Framework for Chemiresistive Sensing. *J. Mater. Chem. A* **2017**, *5*, 16139−16143.
(7) Wäckerlin, C.; Chylarecka, D.; Kleibert, A.; Müller, K.; Iacovita, C.; Nolting, F.; Jung, T. A.; Ballav, N. Controlling Spins in Adsorbed Molecules by a Chemical Switch. *Nat. Commun.* **2010**, *1*, 1−7.
(8) Chakravarty, C.; Mandal, B.; Sarkar, P. Bis(Dithiolene)-Based Metal-Organic Frameworks with Superior Electronic and Magnetic Properties: Spin Frustration to Spintronics and Gas Sensing. *J. Phys. Chem. C* **2016**, *120*, 28307−28319.
(9) Mandal, B.; Sarkar, P. A New Two-Dimensional Metal−Organic Framework with High Spin-Filtering Efficiency. *Phys. Chem. Chem. Phys.* **2015**, *17*, 17437−17444.
(10) Sheberla, D.; Sun, L.; Blood-Forsythe, M. A.; Er, S.; Wade, C. R.; Brozek, C. K.; Aspuru-Guzik, A.; Dincă, M. High Electrical Conductivity in $Ni_3$(2,3,6,7,10,11- Hexaiminotriphenylene)$_2$, a Semiconducting Metal-Organic Graphene Analogue. *J. Am. Chem. Soc.* **2014**, *136*, 8859−8862.
(11) Dou, J. H.; Sun, L.; Ge, Y.; Li, W.; Hendon, C. H.; Li, J.; Gul, S.; Yano, J.; Stach, E. A.; Dincă, M. Signature of Metallic Behavior in the Metal-Organic Frameworks $M_3$(Hexaiminobenzene)$_2$ (M = Ni, Cu). *J. Am. Chem. Soc.* **2017**, *139*, 13608−13611.
(12) Sheberla, D.; Bachman, J. C.; Elias, J. S.; Sun, C. J.; Shao-Horn, Y.; Dincă, M. Conductive MOF Electrodes for Stable Supercapacitors with High Areal Capacitance. *Nat. Mater.* **2017**, *16*, 220−224.


DOI: 10.1021/jacs.9b04822
J. Am. Chem. Soc. 2019, 141, 10475−10480

(13) Feng, D.; Lei, T.; Lukatskaya, M. R.; Park, J.; Huang, Z.; Lee, M.; Shaw, L.; Chen, S.; Yakovenko, A. A.; Kulkarni, A.; Xiao, J.; Fredrickson, K.; Tok, J. B.; Zou, X.; Cui, Y.; Bao, Z. Robust and Conductive Two-Dimensional Metal-Organic Frameworks with Exceptionally High Volumetric and Areal Capacitance. *Nat. Energy* **2018**, *3*, 30−36.
(14) Benmansour, S.; Abhervé, A.; Gómez-Claramunt, P.; Vallés-García, C.; Gómez-García, C. J. Nanosheets of Two-Dimensional Magnetic and Conducting Fe(II)/Fe(III) Mixed-Valence Metal-Organic Frameworks. *ACS Appl. Mater. Interfaces* **2017**, *9*, 26210−26218.
(15) Dong, R.; Han, P.; Arora, H.; Ballabio, M.; Karakus, M.; Zhang, Z.; Shekhar, C.; Adler, P.; Petkov, P. S.; Erbe, A.; Mannsfeld, S. C. B.; Felser, C.; Heine, T.; Bonn, M.; Feng, X.; Cánovas, E. High-Mobility Band-like Charge Transport in a Semiconducting Two-Dimensional Metal−Organic Framework. *Nat. Mater.* **2018**, *17*, 1027−1032.
(16) Zhang, X.; Vieru, V.; Feng, X.; Liu, J.; Zhang, Z.; Na, B.; Shi, W.; Wang, B.; Powell, A. K.; Chibotaru, L. F.; Gao, S.; Cheng, P.; Long, J. R. Influence of Guest Exchange on the Magnetization Dynamics of Dilanthanide Single-Molecule-Magnet Nodes within a Metal-Organic Framework. *Angew. Chem., Int. Ed.* **2015**, *54*, 9861−9865.
(17) Campbell, M. G.; Sheberla, D.; Liu, S. F.; Swager, T. M.; Dincă, M. $Cu_3$(Hexaiminotriphenylene)$_2$: An Electrically Conductive 2D Metal-Organic Framework for Chemiresistive Sensing. *Angew. Chem., Int. Ed.* **2015**, *54*, 4349−4352.
(18) Zhao, M.; Wang, A.; Zhang, X. Half-Metallicity of a Kagome Spin Lattice: The Case of a Manganese Bis-Dithiolene Monolayer. *Nanoscale* **2013**, *5*, 10404−10408.
(19) Zhou, Q.; Wang, J.; Chwee, T. S.; Wu, G.; Wang, X.; Ye, Q.; Xu, J.; Yang, S. W. Topological Insulators Based on 2D Shape-Persistent Organic Ligand Complexes. *Nanoscale* **2015**, *7*, 727−735.
(20) Li, W.; Sun, L.; Qi, J.; Jarillo-Herrero, P.; Dincă, M.; Li, J. High Temperature Ferromagnetism in π-Conjugated Two-Dimensional Metal-Organic Frameworks. *Chem. Sci.* **2017**, *8*, 2859−2867.
(21) Long, J. R.; Williamson, A. S.; Holm, R. H. Dimensional Reduction of $Re_6Se_8Cl_2$: Sheets, Chains, and Discrete Clusters Composed of Chloride-Terminated $[Re_6Q_8]^{2+}$ (Q = S, Se) Cores. *Angew. Chem., Int. Ed. Engl.* **1995**, *34*, 226−229.
(22) Tulsky, E. G.; Long, J. R. Dimensional Reduction: A Practical Formalism for Manipulating Solid Structures. *Chem. Mater.* **2001**, *13*, 1149−1166.
(23) Heinrich, J. L.; Berseth, P. A.; Long, J. R. Molecular Prussian Blue Analogues: Synthesis and Structure of Cubic $Cr_4Co_4(CN)_{12}$ and $Co_8(CN)_{12}$ Clusters. *Chem. Commun.* **1998**, *4*, 1231−1232.
(24) Grange, C. S.; Meijer, A. J. H. M.; Ward, M. D. Trinuclear Ruthenium Dioxolene Complexes Based on the Bridging Ligand Hexahydroxytriphenylene: Electrochemistry, Spectroscopy, and near-Infrared Electrochromic Behaviour Associated with a Reversible Seven-Membered Redox Chain. *Dalton Trans.* **2010**, *39*, 200−211.
(25) Suenaga, Y.; Inada, H.; Inomata, M.; Yamaguchi, R.; Okubo, T.; Maekawa, M.; Kuroda-Sowa, T. Crystal Structure and Characterization of Trinuclear Cobalt(III) Complex with 2,3,6,7,10,11-Hexahydroxytriphenylene. *Chem. Lett.* **2014**, *43*, 562−564.
(26) Hoshino, N.; Akutagawa, T. A Trinuclear Iron(III) Complex of a Triple Non-Innocent Ligand toward Spin-Structured Molecular Conductors. *Chem. - Eur. J.* **2018**, *24*, 19323.
(27) Pierpont, C. G.; Lange, C. W. The Chemistry of Transition Metal Complexes Containing Catechol and Semiquinone Ligands. In *Progress in Inorganic Chemistry*; Wiley, 2007; Vol. *41*, pp 331−442.
(28) Ovcharenko, V. I.; Gorelik, E. V.; Fokin, S. V.; Romanenko, G. V.; Ikorskii, V. N.; Krashilina, A. V.; Cherkasov, V. K.; Abakumov, G. A. Ligand Effects on the Ferro- to Antiferromagnetic Exchange Ratio in Bis(o-Semiquinonato)Copper(II). *J. Am. Chem. Soc.* **2007**, *129*, 10512−10521.
(29) Schweinfurth, D.; Khusniyarov, M. M.; Bubrin, D.; Hohloch, S.; Su, C.-Y.; Sarkar, B. Tuning Spin−Spin Coupling in Quinonoid-Bridged Dicopper(II) Complexes through Rational Bridge Variation. *Inorg. Chem.* **2013**, *52*, 10332−10339.
(30) Barthram, A. M.; Reeves, Z. R.; Jeffery, J. C.; Ward, M. D. Polynuclear Osmium-Dioxolene Complexes: Comparison of Electrochemical and Spectroelectrochemical Properties with Those of Their Ruthenium Analogues. *J. Chem. Soc., Dalton Trans.* **2000**, 3162−3169.
(31) Richardson, D. E.; Taube, H. Mixed-Valence Molecules: Electronic Delocalization and Stabilization. *Coord. Chem. Rev.* **1984**, *60*, 107−129.
(32) Sakamoto, R.; Kambe, T.; Tsukada, S.; Takada, K.; Hoshiko, K.; Kitagawa, Y.; Okumura, M.; Nishihara, H. Π-Conjugated Trinuclear Group-9 Metalladithiolenes With a Triphenylene Backbone. *Inorg. Chem.* **2013**, *52*, 7411−7416.
(33) Sutton, J. E.; Taube, H. Metal to Metal Interactions in Weakly Coupled Mixed-Valence Complexes Based on Ruthenium Ammines. *Inorg. Chem.* **1981**, *20*, 3125−3134.
(34) Robin, M. B.; Day, P. *Adv. Inorg. Chem. Radiochem.* **1968**, *10*, 247−422.
(35) Menage, S.; Vitols, S. E.; Bergerat, P.; Codjovi, E.; Kahn, O.; Girerd, J. J.; Guillot, M.; Solans, X.; Calvet, T. Structure of the Linear Trinuclear Complex Hexakis(Acetato)Bis(2,2′-Bipyridine)-Trimanganese (II). Determination of the J Electron-Exchange Parameter through Magnetic Susceptibility and High-Field Magnetization Measurements. *Inorg. Chem.* **1991**, *30*, 2666−2671.
(36) Kambe, T.; Tsukada, S.; Sakamoto, R.; Nishihara, H. Expanding Family of π-Conjugated Trinuclear Dithiolenes: The Cases of Group 8 (RuII) and 10 (NiII and PtII) Metals. *Inorg. Chem.* **2011**, *50*, 6856−6858.
(37) Liu, J.; Sun, Q. Enhanced Ferromagnetism in a $Mn_3C_{12}N_{12}H_{12}$ Sheet. *ChemPhysChem* **2015**, *16*, 614−620.
(38) Kahn, O. *Molecular Magnetism*; VCH Publishers, Inc., 1993.
(39) Tsukerblat, B. S.; Kuyavskaya, B. Y.; Belinskii, M. I.; Ablov, A. V.; Novotortsev, V. M.; Kalinnikov, V. T. Antisymmetric Exchange in the Trinuclear Clusters of Copper (II). *Theor. Chim. Acta* **1975**, *38*, 131−138.
(40) Cage, B.; Cotton, F. A.; Dalal, N. S.; Hillard, E. a.; Rakvin, B.; Ramsey, C. M. Observation of Symmetry Lowering and Electron Localization in the Doublet-States of a Spin-Frustrated Equilateral Triangular Lattice: $Cu_3(O_2C_{16}H_{23})\cdot 1.2C_6H_{12}$. *J. Am. Chem. Soc.* **2003**, *125*, 5270−5271.
(41) Hagemann, I. S.; Huang, Q.; Gao, X. P. A.; Ramirez, A. P.; Cava, R. J. Geometric Magnetic Frustration in $Ba_2Sn_2Ga_3ZnCr_7O_{22}$: A Two-Dimensional Spinel Based Kagomé Lattice. *Phys. Rev. Lett.* **2001**, *86*, 894−897.
(42) Shores, M. P.; Bartlett, B. M.; Nocera, D. G. Spin-Frustrated Organic-Inorganic Hybrids of Lindgrenite. *J. Am. Chem. Soc.* **2005**, *127*, 17986−17987.


DOI: 10.1021/jacs.9b04822
*J. Am. Chem. Soc.* 2019, 141, 10475−10480